Journal of Alloys and Compounds 606 (2014) 208–213

Contents lists available at ScienceDirect

Journal of Alloys and Compounds

journal homepage: www.elsevier.com/locate/jalcom

Effect of a ZnO buffer layer on the properties of epitaxial ZnO:Ga films deposited on c-sapphire substrate

Zhiyun Zhang [a,*], Chonggao Bao [b], Dawei Yi [a], Bo Yang [c], Qun Li [b], Shuzeng Hou [b], Z.H. Han [d]

[a] School of Materials Science and Engineering, Xi'an University of Science and Technology, Xi'an, Shaanxi Province 710054, PR China
[b] State Key Laboratory for Mechanical Behaviour of Materials, School of Materials Science and Engineering, Xi'an Jiaotong University, Xi'an, Shaanxi Province 710049, PR China
[c] No. 95 Binhai Road, Jiaojiang, Taizhou, Zhejiang Province 318000, PR China
[d] School of Materials Science and Engineering, Xi'an University of Technology, Xi'an, Shaanxi Province 710068, PR China

ARTICLE INFO

Article history:
Received 21 May 2013
Received in revised form 9 September 2013
Accepted 12 February 2014
Available online 21 February 2014

Keywords:
HRTEM
AZO
GZO
Bi-layer film
Stacking faults
Defect density

ABSTRACT

Bi-layer ZnO films with 2 wt.% Al (AZO; ZnO:Al) and 4 wt.% Ga-doped (GZO; ZnO:Ga) were deposited on the non-buffered and buffered c(0001)-sapphire(Al_2O_3) substrates respectively by Pulsed Laser Deposition (PLD). The effect of a ZnO buffer layer on the crystallinity and electrical properties of the GZO thin films was investigated. X-ray Diffraction (XRD) peaks and High Resolution Transmission Electron Microscopy (HRTEM) studies showed that the GZO thin film on a buffered substrate was epitaxially grown with an orientation relationship of $(0001)\,[1\,1\,\bar{2}\,0]_{GZO}||(0001)[1\,1\,\bar{2}\,0]_{Al_2O_3}$. However, GZO thin film on a non-buffered substrate was grown as a monocrystalline hexagonal wurtzite phase with *c*-axis preferred, out-of-plane orientation, and random in-plane orientation. The electrical resistivity of the GZO thin films was improved by introducing a ZnO buffer layer from $2.2 \times 10^{-4}\ \Omega$ cm to $1.2 \times 10^{-4}\ \Omega$ cm, respectively. In a word, it was found in the films that more preferred *c*-axis orientation texture and reduction of the defects such as stacking faults and dislocations, with introducing a ZnO buffer layer.

It was seen that the ZnO buffer layer had a great influence on the orientation and defect density of GZO thin films from X-ray Diffraction (XRD) peaks and High Resolution Transmission Electron Microscopy (HRTEM) images.

1. Introduction

Electronically doped thin films provide vital function in many emerging field. Transparent conducting films (TCO) [1–3], for example, are important in displays, sensors, touch panels, light-emitting diodes, photovoltaic cells, and transparent electronics [4–6]. Recently, optically pumped excitonic lasing of ZnO thin films at room temperature and lasing effect of ZnO nanowire arrays have been observed [7]. Epitaxial growth of ZnO has been accomplished on Si [8] and mainly on c-sapphire substrate [9–12] using various techniques. ZnO is an n-type wide band gap semiconductor, and its electrical conductivity is dominated by Zn interstitial atoms and oxygen vacancies [13]. However, un-doped ZnO thin films show high resistivity due to low carrier concentration in the films. Therefore extrinsic doping of ZnO by substitution of group III element [14,15] for ZnO, or group VII element [16] for O are also well investigated. Among these impurities, Ga is considered as the most promising dopant element for the following reasons. Ga is less reactive and more resistant to oxidation and has an ionic radius similar to that of Zn ions, which minimizes lattice deformations in the ZnO crystal structure even at high doping concentrations, as compared to the action of other impurities. When ZnO is heavily doped with Al or Ga, yet, the resistivity increases because of the depletion of carrier concentration due to reduction of oxygen vacancies in impurity-doped ZnO and increase of the neutral impurity scattering [17].

Because of this development, it is essential to grow high quality epitaxial impurity-doped ZnO thin films which can employ ZnO film with high performance and reliability, since polycrystalline impurity-doped ZnO films have many dislocations and stacking faults, non-crystallinity region and grain boundaries, which result in interference of transmitted light and the mobility of carriers in the film [18,19]. Epitaxial impurity-doped ZnO films have been prepared by a lot of techniques such as RF magnetron sputtering [20], pulsed laser deposition [13], metal organic chemical vapor deposition [21] and molecular beam epitaxy [22] on Al_2O_3 substrates. However, it is reported that impurity-doped ZnO films,

* Corresponding author. Address: School of Materials Science and Engineering, Xi'an University of Science and Technology, 58 Yanta Road, Xi'an, Shaanxi Province 710054, PR China. Tel./fax: +86 29 85587060.
E-mail address: zhangzhiyun01@163.com (Z. Zhang).

http://dx.doi.org/10.1016/j.jallcom.2014.02.062
0925-8388/

which are employed not inducing a buffer layer cannot be grown epitaxially or that the doping effect deteriorates when the impurity doping concentration gets higher than 3 wt%.

It is well known that extended defects with high density such as symmetrical tilt grain boundaries, dislocations and stacking faults are included in ZnO thin films and extended defects play an important role in electrical properties of semiconductors [23]. For example, these defects may introduce energy levels in the band gap. In this state, the quantum efficiency and the lifetime of devices can be affected [24]. These different extended defects could be induced in ZnO thin films by residual stress due to the lattice mismatch between ZnO films and the substrate and the divergence of the thermal expansion coefficients. The electrical and optical properties of ZnO films are influenced by the microstructures related to the grain boundaries of the films. Especially, some grain boundaries have lower energy and specific atomic configurations at the grain boundary core that are different from the coordination of atoms in a single crystal. It is well known that grain boundaries in polycrystalline films tend to enlarge the electrical resistivity of the films, but impurity-doped ZnO single crystal films which can eliminate the grain boundaries effects on the properties of thin films, have been little investigated yet.

As everybody knows that impurity-doped ZnO films also have a hexagonal wurtzite structure same as ZnO film and grow along *c*-axis in order to minimize the surface energy. Inspite of great researches have characterized the electrical properties and microstructures of impurity-doped ZnO thin films, observation by HRTEM on an atomic level of the crystal structure and the atomic arrangement of epitaxial GZO thin films on c-sapphire substrates predeposited by ZnO homo-buffer layer has been little investigated yet.

Therefore, In this paper we have attempted to prepare a high quality epitaxial GZO thin films on a ZnO buffered and non-buffered c-sapphire substrates with a high doping concentration of 4 wt% Ga and 2 wt% Al using pulsed laser deposition. The effect of a ZnO buffer layer on the microstructural and electrical properties of epitaxial GZO thin films deposited on the c-sapphire substrates by PLD was studied in details. The GZO thin films deposited on ZnO buffered c-sapphire and non-buffered c-sapphire were characterized by HRTEM in order to clarify exactly the nanostructural changes of GZO thin films on an atomic level.

2. Experimental procedure

The 800 nm thick GZO thin films were prepared on the ZnO buffered and non-buffered c-sapphire substrates by using PLD method. The pure ZnO, 4 wt% Ga-doped ZnO and 2 wt% Al-doped ZnO targets were prepared by the conventional solid-state reaction method. Before deposited the ZnO buffer layer and GZO thin films, the c-sapphire substrates were cleaned ultrasonically using acetone, methanol, isopropyl alcohol, and deionized water for 10 min continuously. Then the cleaned substrates were dried by blowing with high purity N_2 (99.999%) gas. The surface of one c-sapphire substrate was predeposited by 20 nm ZnO homo-buffer layer at 500 °C with a wavelength of 248 nm and a pulse duration of 25 ns on a ZnO target. The other c-sapphire substrate did not deposited buffer layer. The AZO/GZO layers were deposited at 500 °C with a wavelength of 248 nm and a pulse duration of 25 ns on a AZO and GZO targets. Following samples with a ZnO buffer layer and non-buffer layer were investigated in this work: 20-nm-ZnO buffer layer/750-nm-GZO/50-nm-AZO and 800-nm-GZO/50-nm-AZO.

The microstructural properties of GZO thin films were analyzed with X-ray Diffraction (XRD) which uses a Cu Kα radiation (λ = 0.1541 nm). The resistivity, carrier concentration and carrier mobility of GZO thin films were measured using Accent HL5500 Hall system with a four-point probe. Before the Hall measurement, the ohmic contact of films with aluminum metal contacts was confirmed. The thin films were analyzed by HRTEM to investigate the crystal structure, defect density and atomic arrangement. The samples for the cross-sectional TEM measurements were prepared by gluing the film, cutting to slices followed by mechanical polishing, dimpling and ion-milling. For a cross-sectional TEM sample Bright-Field (BF) TEM image, Selected Area Electron Diffraction (SAED) pattern and the HRTEM image were obtained with TEM (JEOL, JEM-2100F) operated at 200 kV with a high-resolution pole piece. The Fast Fourier Transform (FFT) and Fourier filtered HRTEM images were obtained by Gatan Digital Micrograph software.

3. Results and discussion

3.1. Structural characterization

Fig. 1 shows XRD patterns of non-buffered and buffered GZO thin films, respectively. The XRD patterns showed that the peaks from the ZnO (0002) planes can be observed in all the films without any other peaks from other phases, indicating that all the films are pure ZnO phase with highly *c*-axis out-of-plane orientation. The appearance of only the (0002) peak indicates that all samples have a preferred [0001] orientation owing to the lowest surface free energy of this orientation [25]. Especially, the ZnO (0002) peaks are located differently at 34.30° and 34.40° for the non-buffered and buffered films. The values of full width at half maximum (FWHM) for the two samples are 0.374 and 0.324, respectively. They are illustrated in Table. 1. The value of FWHM of buffered film is lower than that of non-buffered film and the intensity of (0002) peak of buffered film is higher than that of non-buffered film, which results in that the buffered film has a more preferential orientation of the [0001] direction. The lattice spacings (d_{0002}) of non-buffered film and buffered film are 0.2612 nm and 0.2604 nm, as determined from the Bragg equation respectively. Although the $d_{(0002)}$ value of the non-buffered film is larger than that of the ZnO bulk (0.2603 nm), the value of the buffered film is almost equal to that of the ZnO bulk. This behavior was acquired in previous works [26,27]. The shifting of 2θ of (0002) plane can be assigned to define the extent of lattice strain along *c*-axis direction. According to Bragg's law ($n\lambda = 2d \sin\theta$), a shifting of 2θ results from the change of lattice parameter d when λ keeps at constant. As shown in Table 1, 2θ of the (0002) plane of the non-buffered film shifts to lower angle (34.30°) resulting from the increase of lattice parameter $d_{(0002)}$ according to Bragg's law. It can be explained by

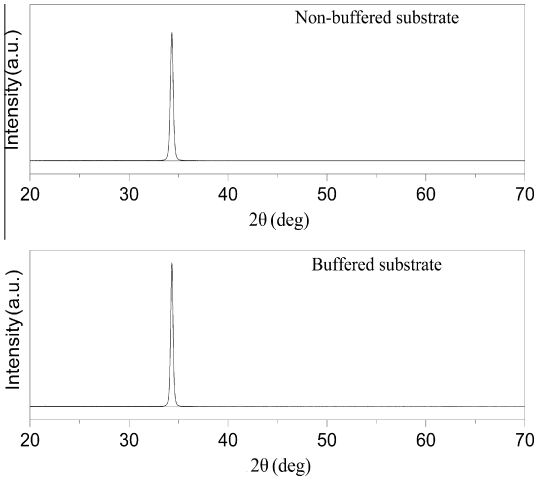

Fig. 1. XRD patterns of GZO thin films deposited at non-buffered c-sapphire substrate and buffered c-sapphire substrate. (b) The FWHMs and diffraction angles of films grown on non-buffered c-sapphire substrate and buffered c-sapphire substrate.

Table 1
The FWHMs and diffraction angles of films grown on non-buffered c-sapphire substrate and buffered c-sapphire substrate.

Deposition condition	Diffraction angles of films (°)	FWHM
Film deposited on non-buffered substrate	34.3	0.374
Film deposited on buffered substrate	34.4	0.324

the tensile strains along *c*-axis direction. But the 2θ of the (0002) plane of the buffered film shifts to the angle (34.40°). It is almost equal to the ZnO bulk materials. The non-buffered film was directly deposited at c-sapphire substrate, which may have many interface defects owing to the lattice difference of ZnO and c-sapphire, But the crystallinity of the buffered film was improved, because the GZO film was deposited at a ZnO buffer layer so that they can attain the thermodynamical equilibrium sites. The XRD patterns for the non-buffered film and the buffered film show that the two kinds of thin films have a strong *c*-axis orientation due to the lowest surface free energy of (0002) plane [25].

It is well known that the crystal structure of impurity-doped ZnO maintains the wurtzite structure [20,28]. that is to say, impurity atoms are replaced to the Zn^{2+} sites keeping the structure of ZnO. ZnO usually has a wurtzite structure, which can be described by the stacking of close-packed double layers of (0002) planes in the [0001] direction [29]. The typical and perfect wurtzite stacking sequence is . . .AaBbAaBb. . . The perfect zinc blende structure can be attained through the stacking sequence of . . .AaBbCcAaBbCc. . . The wurtzite structure composes only hexagonal bonds, but the zinc blende structure contains cubic bonds only. Concerning the crystal growth, ZnO would grow along the *c*-axis perpendicular to (0002) plane due to the (0002) plane having the lowest surface free energy. The packed sequence of each atomic layer in wurtzite ZnO can be observed in the $[2\bar{1}\bar{1}0]$ zone axis. As shown in Fig. 2 [30], the atomic arrangement alternately stacked along the [0001] direction can be exactly viewed in the $[2\bar{1}\bar{1}0]$ zone axis. Consequently, the epitaxial films in our work observed along the $[2\bar{1}\bar{1}0]$ direction can be also recognized clearly on atomic level. A misfit introduced into the perfect wurtzite stacking sequence will produce a basal-plane stacking fault in wurtzite ZnO. All of the basal-plane stacking faults are found to have very low formation energy [29]. The existence of high concentration stacking faults could result in embedded zinc blende ZnO surrounded by wurtzite ZnO. The zinc blende regions will behave like trap centers to the free carriers. These defects will obstruct the migration of carriers.

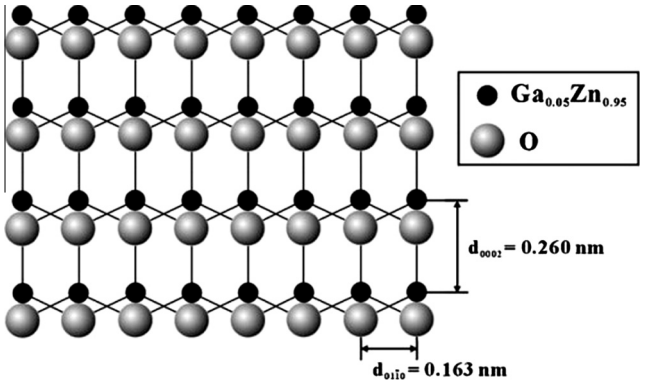

Fig. 2. The atomic arrangement of impurity-doped ZnO film viewed along the $[2\bar{1}\bar{1}0]$ zone axis.

Fig. 3(a) and (c) shows cross-sectional bright-field TEM patterns of GZO thin films deposited at non-buffered substrate and buffered substrate, respectively. Fig. 3(b) and (d) presents corresponding selected area electron diffraction (SAED) micrographs obtained from the film and substrate interface. Dense monocrystal GZO thin films grown on non-buffered substrate and buffered substrate are obtained, as shown in Fig. 3(b) and (d). The vertical straight dark fringes defects in Fig. 3(a) and (c) can be attributed to threading dislocations which might initiate from a large lattice mismatch (18.3%) between ZnO film and c-sapphire substrate. In the meantime, it is observed that the interface between GZO thin film and the substrate are very sharp without any indication of interfacial

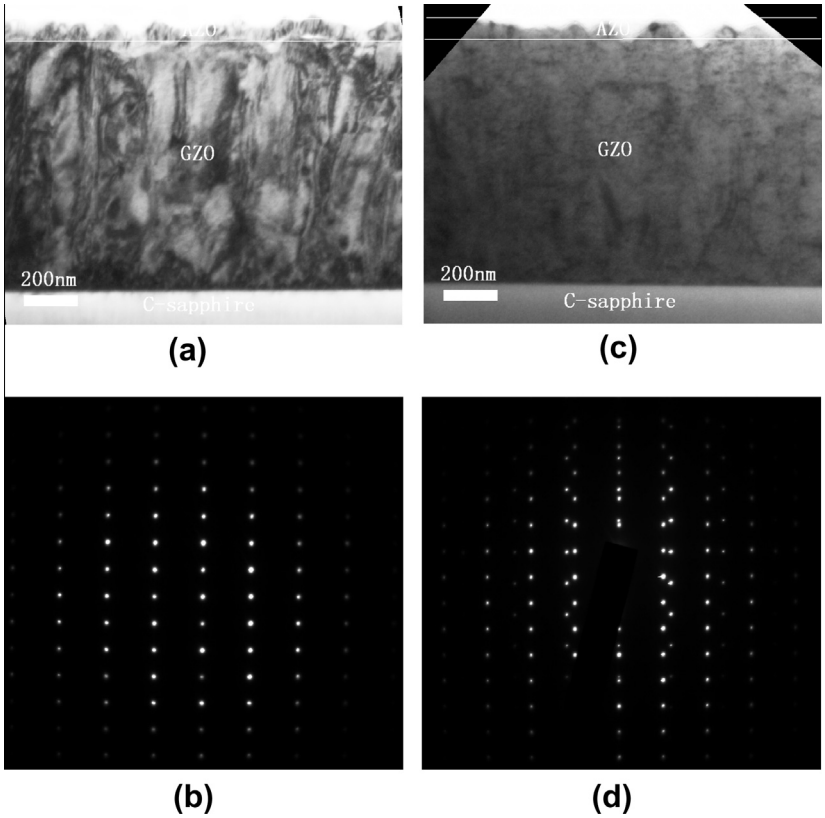

Fig. 3. Cross-sectional bright-Field TEM images and SAED patterns of the GZO thin films deposited at (a, b) non-buffered substrate and (c, d) buffered substrate, respectively.

reaction or any formation of interfacial compounds. None of the distinct grain boundaries, which are typically observed in polycrystalline thin films, are observed in the film in Fig. 3(a) and (c). The SAED pattern in the Fig. 3(d) shows a typical pattern from the epitaxial film and the substrate interface. The indexing of this pattern shows that GZO thin film is grown epitaxially with an orientation relationship of $(0002)[1\,1\bar{2}\,0]_{AZO/GZO}||(0002)[1\,1\bar{2}\,0]_{Al2O3}$. This result is quite consistent with the XRD results shown in Fig. 1. Meanwhile the SAED interface pattern of non-buffered film shown in Fig. 3(b) shows a set of diffraction spots belonging to ZnO. It maybe that orientation of non-buffered film and substrate is abnormity. It is obvious from Fig. 3(a) that there be exist higher density of threading dislocations throughout the film. Moreover the lattice mismatch, the low mobility of substitutional impurity atoms could also contribute to the density of dislocations. Besides the threading dislocations in Fig. 3(a) and (c), a high density of partial dislocation loop associated with a stacking fault also exists in the thin films, as can be seen in the representative Fourier filtered HRTEM image in Fig. 4. The formation of a stacking fault can be explained by the condensation of point defects such as zinc interstitials, impurity (Al, Ga) interstitials or oxygen vacancies. This contrast indicates that the thin film deposited on buffered substrate has better crystallinity than that of thin film deposited on non-buffered substrate, even if they are both single crystal thin films.

So as to designate the as-grown defects in the two kinds of films, we did HRTEM measurements. Any stacking fault can easily be discerned because of a change in the stacking sequence of close-packed planes along the [0001] growth direction. Two low-energy stacking faults with distinct stacking sequences and bounding partial dislocations exist in the hexagonal wurtzite lattice crystal structure. The Fourier-filtered image of Bright-Field HRTEM shown in Fig. 5 is a representative as-grown single layer stacking fault. The black straight line points the position of the stacking fault. The inset of the figure is an illustration drafting of the atomic site, in which capital and small letter corresponds to zinc and oxygen atom respectively. The atom stack sequence is ...AaBbAaBb|CcBbCcBb..., which is agreeing with the research consequence employed by the first principles [29]. The symbol " | " marks the position where the violation of the stacking regulation sets out.

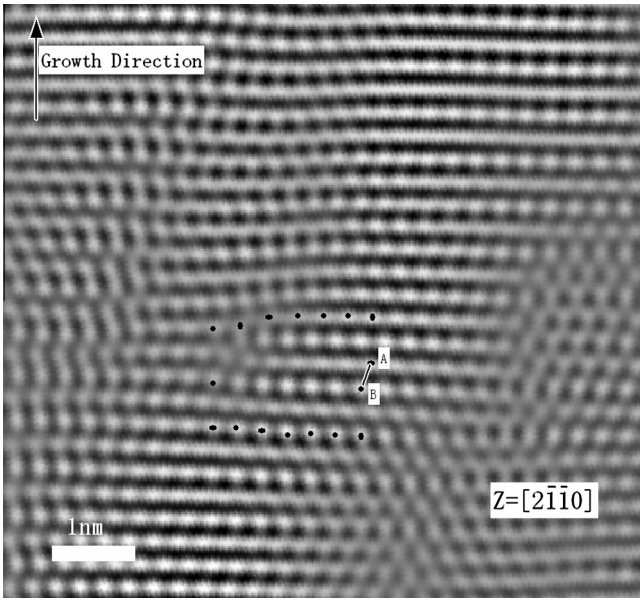

Fig. 4. Fourier-filtered HRTEM image of an end-on partial dislocation from the film deposited at non-buffered c-sapphire substrate.

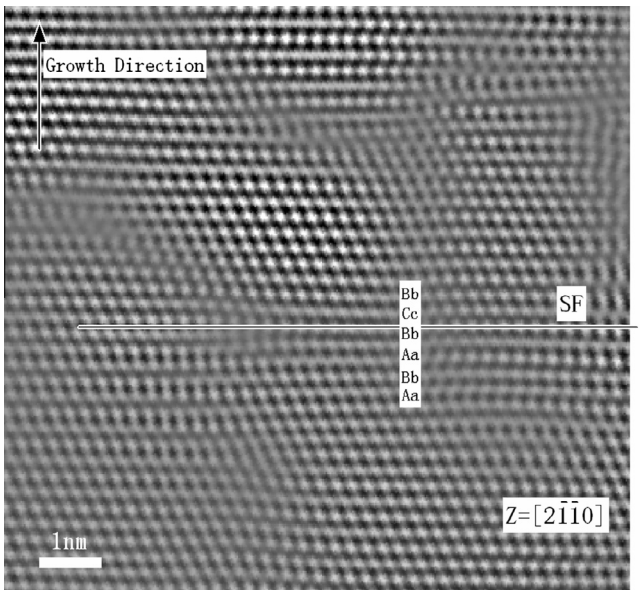

Fig. 5. Fourier-filtered HRTEM image of stacking faults with Burger vector lying in the (0002) plane.

The upper and lower sections are still perfect wurtzite crystal structure but the mistake sequence layer has a relatively translation of $\sqrt{3}/3$ a along the $[01\bar{1}0]$ direction in the (0002) plane. The movement vector is $b = 1/3[01\bar{1}0]$. This kind of vector does not have a perpendicular component along the [0001] direction, as demonstrated by AC in Fig. 6. Such stacking faults may have its origins in incoherent boundaries between nearing columnar grains during the growth. Another low energy stacking fault is generated by condensation of interstitials or vacancies, which results in a losing or an extra (0002) plane in the crystal lattice. Since the condensation procedure brings on high-energy defects, a Shockley partial dislocation loop is likely to be formed in the defective region [31]. In the edge of this kind of stacking fault, a Shockley partial dislocation accompanied it. The Fourier-filtered image of Bright-Field HRTEM of the partial dislocation accompanying a stacking fault is illustrated in Fig. 4, and the white line in the plot illustrates the circuit of Burgers vector analysis. The Burgers vector of the partial dislocations is $b = 1/6[02\bar{2}\bar{3}]$ shown in Fig. 6, which can be breaked up to b_1 and b_2 two kinds of Burgers vector. Vector $b_1 = 1/2[000\bar{1}]$ corresponded to spatial dislocation along the $[000\bar{1}]$ direction and vector $b_2 = 1/3[01\bar{1}0]$ corresponded to spatial dislocation along the $[01\bar{1}0]$ direction. Most stacking faults in our experiment are characterized through an additional (0002) plane (marked in Fig. 4), which demonstrates that the stacking faults are chiefly formed by the deposition of interstitials. If the solubility of impurity is exceeded, the deposition of impurity interstitials arises. But it should be stress that the generation of a stacking fault demands the precipitation of a double layer including impurity and oxygen atoms. If impurity interstitials precipitate in the lattice, oxygen atoms must diffuse from the adjacent lattice to build a complete (0002) double layer. The result of high stacking fault density is demonstrative of high point defects concentrations such as vacancies and interstitials. A careful adjustment of the concentration of doped impurity appears to be essential to control the point defects density and understand its effect on the electrical properties of impurity-doped ZnO.

Fig. 7(a and b) shows the HRTEM and corresponding Fourier-filtered image of the film deposited at non-buffered substrate. Fig. 7(c and d) shows the HRTEM and corresponding Fourier-filtered image of the film deposited at buffered substrate. The interplanar spacing distance of the (0002) of the film deposited on non-buffered substrate is 0.2611 nm, and the non-buffered film

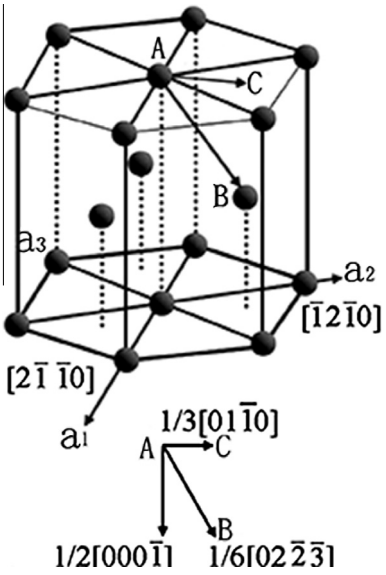

Fig. 6. A schematic illustration of possible Burgers vector AB and AC in impurity-doped ZnO.

receives a tensile stress along the c-axis. The interplanar distance of the (0002) of buffered film is 0.2604 nm. The results are in reasonable agreement with the XRD analysis. As well known, the number of microstructural defects has a great effect on the electrical properties of thin films, the stacking faults and other defects acting as a barrier of carrier migration could be easily observed in non-buffered substrate during the thin film growth. On the contrary, the film grown at buffered substrate has comparatively homogeneous atomic arrangement. There are more stacking faults and defects in the film deposited at non-buffered substrate than that of film deposited at buffered substrate, as shown in Fig. 7(b and d). Therefore, the electrical properties of thin film can be improved by the reduction of stacking faults and other defects through introducing a ZnO homogeneous buffer layer. Because carrier mobility is defect dependent, which indicates that the formation of 2DEG is dependent on the material's defect density. We will study the AZO/GZO two dimensional electron gases heterostructure in future study.

Table 2
A list of values of electrical resistivity, carrier concentration and mobility of films deposited at different conditions.

Deposition condition	Hall mobility ($cm^2/V\,s$)	Electron concentration ($\times10^{20}/cm^{-3}$)	Resistivity ($\times10^{-4}\,\Omega\,cm$)
Film grown on non-buffered substrate	18	16	2.2
Film grown on buffered substrate	32	16	1.2

3.2. Electrical properties

Table 2 shows the electrical resistivity, carrier concentration, and mobility of the GZO thin films deposited at non-buffered substrate and buffered substrate. The electrical resistivity, carrier concentration and mobility of the film deposited at non-buffered substrate are $2.2 \times 10^{-4}\,\Omega\,cm$, $16 \times 10^{20}\,cm^{-3}$ and $18\,cm^2\,V^{-1}\,s^{-1}$,

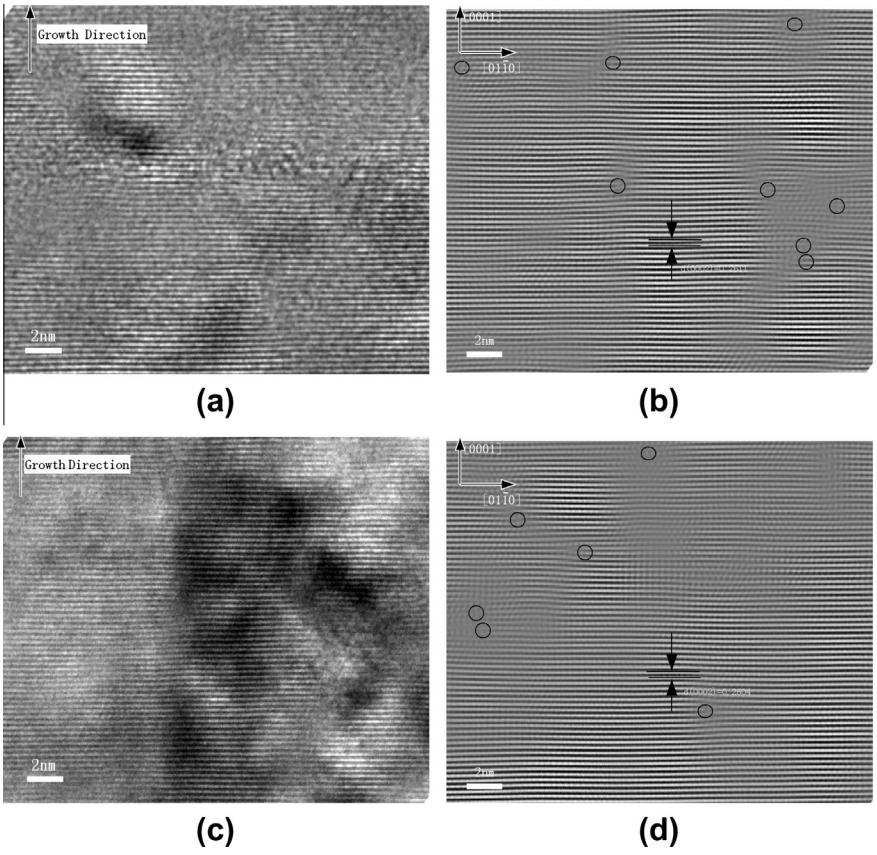

Fig. 7. (a) HRTEM image from the film deposited at non-buffered c-sapphire. (b) Fourier-filtered image of (a) containing many stacking faults. (c) HRTEM image from the film deposited at buffered c-sapphire. (d) Fourier-filtered image of (c) containing a few stacking faults. The white circles mark partial dislocations, which terminate stacking faults.

respectively. The electrical properties of the GZO thin films deposited at buffered substrate, which are $1.2 \times 10^{-4}\,\Omega\,cm$, $16 \times 10^{20}\,cm^{-3}$ and $32\,cm^2\,V^{-1}\,s^{-1}$, represent an improvement over that of the film grown at non-buffered substrate.

It is reported that the defects and grain boundaries in impurity-doped ZnO thin films have a harmful effect on their electrical properties. The impurity will substitute for Zn sites and can act as the scattering centers for carrier transport which results in reduction of the mean free path and mobility of carriers. Therefore, it is believed that our experimental results, which showed improved electrical characteristics of the GZO thin films deposited at a buffered substrate, as compared to the thin film at a non-buffered substrate, can be attributed to the improved crystal quality, less dislocations and stacking faults, as shown in Fig. 3(a,c), Fig. 7(a,c).

4. Conclusions

In summary, the microstructures of epitaxial GZO thin films were characterized by XRD and TEM study. The bi-layer thin films deposited by PLD were epitaxial growth. However, the thin film deposited at buffered substrate had much lower resistivity and higher mobility than that deposited at non-buffered substrate. Lower resistivity and higher mobility can be contributed to improved characteristics of *c*-axis orientation texture and the reduction of crystal defects, resulted from introducing a ZnO buffer layer.

Acknowledgements

This work was supported partially by Scientific Research Program Funded by Shaanxi Provincial Education Department (Program No. 2013JK0919) and partially by the Research Foundation of Xi'an University of Science and Technology (Program No. 2013QDJ026, 2012QDJ034 and 201202).

References

[1] S. Kim, J. Seo, H.W. Jang, J. Bang, W. Lee, T. Lee, J.M. Myoung, Appl. Surf. Sci. 255 (2009) 4616–4622.
[2] S.M. Park, T. Ikegami, K. Ebihara, P.K. Shin, Appl. Surf. Sci. 253 (2006) 1522–1527.
[3] I. Volintiru, M. Creatore, M.C.M. van de Sanden, J. Appl. Phys. 103 (2008).
[4] B.H. Kong, W.S. Han, Y.Y. Kim, H.K. Cho, J.H. Kim, Appl. Surf. Sci. 256 (2010) 4972–4976.
[5] M. Kumar, T.H. Kim, S.S. Kim, B.T. Lee, Appl. Phys. Lett. 89 (2006).
[6] D.P. Norton, S.J. Pearton, A.F. Hebard, N. Theodoropoulou, L.A. Boatner, R.G. Wilson, Appl. Phys. Lett. 82 (2003) 239–241.
[7] M.H. Huang, S. Mao, H. Feick, H.Q. Yan, Y.Y. Wu, H. Kind, E. Weber, R. Russo, P.D. Yang, Science 292 (2001) 1897–1899.
[8] Z.Q. Fang, B. Claflin, D.C. Look, L.L. Kerr, X.N. Li, J. Appl. Phys. 102 (2007) 023714.
[9] D. Gerthsen, D. Litvinov, T. Gruber, C. Kirchner, A. Waag, Appl. Phys. Lett. 81 (2002) 3972–3974.
[10] J.H. Lim, D.K. Hwang, H.S. Kim, J.Y. Oh, J.H. Yang, R. Navamathavan, S.J. Park, Appl. Phys. Lett. 85 (2004) 6191–6193.
[11] Q.B. Ma, Z.Z. Ye, H.P. He, S.H. Hu, J.R. Wang, L.P. Zhu, Y.Z. Zhang, B.H. Zhao, J. Cryst. Growth 304 (2007) 64–68.
[12] N. Nishimoto, T. Yamamae, T. Kaku, Y. Matsuo, K. Senthilkumar, O. Senthilkumar, J. Okamoto, Y. Yamada, S. Kubo, Y. Fujita, J. Cryst. Growth 310 (2008) 5003–5006.
[13] R.C. Scott, K.D. Leedy, B. Bayraktaroglu, D.C. Look, Y.H. Zhang, Appl. Phys. Lett. 97 (2010) 072113.
[14] J. Meyer, P. Gorrn, S. Hamwi, H.H. Johannes, T. Riedl, W. Kowalsky, Appl. Phys. Lett. 93 (2008).
[15] K.J. Chen, T.H. Fang, F.Y. Hung, L.W. Ji, S.J. Chang, S.J. Young, Y.J. Hsiao, Appl. Surf. Sci. 254 (2008) 5791–5795.
[16] Y.H. Kim, J. Jeong, K.S. Lee, J.K. Park, Y.J. Baik, T.Y. Seong, W.M. Kim, Appl. Surf. Sci. 256 (2010) 5102–5107.
[17] T. Yamada, H. Makino, N. Yamamoto, T. Yamamoto, J. Appl. Phys. 107 (2010) 123534.
[18] L. Ke, S.C. Lai, J.D. Ye, V.L. Kaixin, S.J. Chua, J. Appl. Phys. 108 (2010) 084502.
[19] D.H. Kim, S.H. Lee, G.H. Lee, H.B. Kim, K.H. Kim, Y.G. Lee, T.H. Yu, J. Appl. Phys. 108 (2010) 023520.
[20] S.W. Shin, K.U. Sim, S.M. Pawar, A.V. Moholkar, I.O. Jung, J.H. Yun, J.H. Moon, J.H. Kim, J.Y. Lee, J. Cryst. Growth 312 (2010) 1551–1556.
[21] J.F. Su, C.H. Zang, C.X. Cheng, Q.A. Niu, Y.S. Zhang, K. Yu, Appl. Surf. Sci. 257 (2010) 160–164.
[22] S. Yang, B.H. Lin, W.R. Liu, J.H. Lin, C.S. Chang, C.H. Hsu, W.F. Hsieh, Cryst. Growth Des. 9 (2009) 5184–5189.
[23] J.W. Lee, S.K. Han, S.K. Hong, J.Y. Lee, T. Yao, J. Cryst. Growth 310 (2008) 4102–4109.
[24] D.C. Look, C. Coskun, B. Claflin, G.C. Farlow, Physica B 340 (2003) 32–38.
[25] P. Pant, J.D. Budai, J. Narayan, Acta Mater. 58 (2010) 1097–1103.
[26] J.H. Lee, Y.Y. Kim, H.K. Cho, J.Y. Lee, J. Cryst. Growth 311 (2009) 4641–4646.
[27] J.W. Shin, J.Y. Lee, Y.S. No, T.W. Kim, W.K. Choi, J. Appl. Phys. 100 (2006) 013526.
[28] Z.F. Liu, F.K. Shan, Y.X. Li, B.C. Shin, Y.S. Yu, J. Cryst. Growth 259 (2003) 130–136.
[29] Y.F. Yan, G.M. Dalpian, M.M. Al-Jassim, S.H. Wei, Phys. Rev. B 70 (2004) 193206.
[30] Y.J. Park, H.N. Kim, H.H. Shin, Appl. Surf. Sci. 255 (2009) 7532–7536.
[31] J. Iqbal, X.F. Liu, H.C. Zhu, Z.B. Wu, Y. Zhang, D.P. Yu, R.H. Yu, Acta Mater. 58 (2010). 1116-1116.